Theoretical Study on Reaction Mechanism of the Methylidyne Radical with Nitrogen Dioxide

Yu-guo Tao,* Yi-hong Ding, Ze-sheng Li, Xu-ri Huang, and Chia-Chung Sun

State Key Laboratory of Theoretical and Computational Chemistry, Institute of Theoretical Chemistry, Jilin University, Changchun 130023, People's Republic of China

Received: October 10, 2000; In Final Form: January 9, 2001

The complex singlet potential energy surface of the $CHNO_2$ system is investigated at the B3LYP and CCSD(T) (single-point) levels in order to explore the possible reaction mechanism of CH radical with NO_2. Twenty-five minimum isomers and 50 transition states are located. Possible energetically allowed reaction pathways leading to various low-lying dissociation products are obtained. Starting from the very energy rich reactant **R** CH + NO_2, the side-attack adduct $HCNO_2$ (**1**) is first formed followed by oxygen-shift almost barrierlessly to give *cis*-OC(H)NO (**2**) and then to *trans*-OC(H)NO (**2′**). Subsequently, the most favorable channel is direct dissociation of **2** and **2′** to product $\mathbf{P_1}$ HCO + NO. The other two much less favorable channels are direct dissociation of **2′** to product $\mathbf{P_2}$ HNO + CO or isomerization of **2′** to a complex HON···CO (**21**) that easily dissociates to product $\mathbf{P_3}$ HON + CO. The large exothermicity released in these processes further drives the three products $\mathbf{P_1}$, $\mathbf{P_2}$, and $\mathbf{P_3}$ to take secondary dissociation to the final product $\mathbf{P_{12}}$ H + CO + NO. The pathways leading to other dissociation products such as NH + CO_2, OH + NCO and HNCO + O, however, are even much less competitive either due to thermodynamical or kinetic factors. A notable finding is that product $\mathbf{P_3}$ HON + CO, which was completely ignored in previous experiments, should be considered in evaluation of the final product yields. The present calculations can excellently explain the experimental result of a very recent diode laser study of the title reaction.

1. Introduction

The methylidyne radical, CH, is believed to play an important role in the prompt-NO formation mechanism and in the NO-reburning process.[1] Nitrogen oxides, NO_x, are among the major atmospheric pollutants released by combustion process. One way to minimize their harmful effects is to chemically reduce them before their release in the atmosphere by the reburning of combustion products in an excess of hydrocarbon.[2] Kinetic studies have been performed on several CH plus NO_x reactions, i.e., CH + NO,[3] CH + N_2O,[4] and CH + NO_2.[5,6] The former two reactions have also been the subject of theoretical investigations.

In 1982, Wagal et al.[5] measured the total rate constant of the reaction CH + NO_2 and obtained that $k = 1.67 \pm 0.11 \times 10^{-10}$ cm^3 $molecule^{-1}s^{-1}$ at 298 K. In 1998, Rim and Hershberger[6] reported the direct measurements of the product branching ratios at 296 K using multiphoton photolysis of $CHBr_3$ at 248 nm followed by time-resolved infrared diode laser products detection. They detected CO, NO, and CO_2 in significant yields, while DCN (from $CDBr_3$), N_2O, HCNO, and HNCO in undetectably low yields. On the basis of consideration of product yields and secondary chemistry, they found that the major product channel is H + CO + NO or HNO + CO, which together account for 92 ± 4% of the total rate constant, whereas the minor product channel is HCO + NO, accounting for 8 ± 4%.

There still remain some unresolved problems of the important radical reaction CH + NO_2 based on Rim and Hershberger's experiment.[6] First, it seems surprising that the very low-lying products NH + CO_2 (−644.2 kJ/mol), HCN + O_2 (−492.1 kJ/mol), HNCO + O (−479.7 kJ/mol), and OH + NCO (−456.9 kJ/mol) were not detected. Second, the observed NO yield is higher than can be accounted for by the title reaction. Third, the measured product branching ratios were influenced by several secondary reactions, which make the actual mechanism of the title reaction somewhat unclear. To explain their experimental result, Rim and Hershberger proposed a possible mechanism, i.e., CH could bind to NO_2 via either the nitrogen atom or an oxygen atom, forming an $HCNO_2$ or HCONO complex, respectively. The $HCNO_2$ complex might rearrange to the HCONO complex via CH migration from the nitrogen to a terminal oxygen atom. The HCONO complex then could dissociate to product HCO + NO or rearrange to CON(H)O that could dissociate to product HNO + CO. Either of these product channels contains enough energy to further dissociate to product H + CO + NO. However, without the knowledge of the detailed potential energy surface, it is surely difficult to discuss the mechanism of this reaction. In fact, Rim and Hershberger stated that "clearly, detailed ab initio calculations are needed to better understand characterize these reaction pathways". Unfortunately, we are not aware of any ab initio calculations on this important reaction.

Therefore, due to the importance of the title reaction and the rather limited knowledge about its reaction mechanism, we decide to carry out a systematic theoretical study. A detailed singlet potential energy surface (PES) is explored by means of density functional theory (DFT-B3LYP) and coupled cluster [CCSD(T)] (single-point) methods. Possible reaction pathways leading to various energetically accessible products are obtained. Finally, the mechanism of the title reaction is established to interpret the diode laser study of Rim and Hershberger.

2. Computational Methods

All computations are carried out using the GAUSSIAN98 program package.[7] The optimized geometries and harmonic

10.1021/jp003717h CCC: $20.00
Published on Web 03/14/2001

TABLE 1: Total (au) and Relative Energies in Parentheses (kcal/mol) as Well as Those Including Zero-Point Vibration Energies (kcal/mol) of the Reactant and Products for the CH + NO_2 Reaction

species	B3LYP/6-311G(d,p)	CCSD(T)/6-311G(d,p)	CCSD(T)/6-311G(d,p) +ZPVE	experimental reaction heats[a]
R CH + NO_2	−243.624 693 1 (0.0)	−243.062 567 6 (0.0)	0.0	
P_1 HCO + NO	−243.813 297 3 (−118.4)	−243.255 641 5 (−121.2)	−119.7	−118.0
P_2 HNO + CO	−243.855 146 3 (−144.6)	−243.309 380 6 (−154.9)	−152.5	−152.7
P_3 HON + CO	−243.790 003 4 (−103.7)	−243.239 941 9 (−111.3)	−109.3	
P_4 ^{1}NH + CO_2	−243.795 556 2 (−107.2)	−243.248 302 6 (−116.6)	−114.1	
P_4' ^{3}NH + CO_2	−243.878 197 1 (−159.1)	−243.323 209 7 (−163.6)	−161.1	−154.1
P_5 HNCO + ^{1}O	−243.716 214 2 (−57.4)	−243.176 748 1 (−71.6)	−67.7	
P_5' HNCO + ^{3}O	−243.818 351 7 (−121.5)	−243.260 727 3 (−124.3)	−120.4	−114.8
P_6 HCNO + ^{1}O	−243.605 851 4 (11.8)	−243.063 857 3 (−0.8)	2.2	
P_6' HCNO + ^{3}O	−243.707 988 9 (−52.3)	−243.147 836 5 (−53.5)	−50.5	−48.7
P_7 HCN + $^1O_2$	−243.754 625 4 (−81.5)	−243.208 753 3 (−91.7)	−88.5	
P_7' HCN + $^3O_2$	−243.816 808 8 (−120.6)	−243.257 881 8 (−122.3)	−119.1	−117.7
P_8 NCO + OH	−243.804 530 7 (−112.8)	−243.240 833 6 (−111.9)	−109.8	−109.3
P_9 CNO + OH	−243.703 790 2 (−49.6)	−243.140 234 3 (−48.7)	−47.4	−42.8
P_{10} CN + HO_2	−243.687 275 4 (−39.3)	−243.130 662 2 (−42.7)	−40.3	−45.5
P_{11} HNC + $^1O_2$	−243.731 063 9 (−66.7)	−243.184 161 2 (−76.3)	−73.6	
P_{11}' HNC + $^3O_2$	−243.793 179 8 (−105.7)	−243.232 989 7 (−106.9)	−104.2	−100.2
P_{12} H + CO + NO	−243.775 093 5 (−94.4)	−243.233 692 5 (−107.4)	−110.9	−102.8

[a] Reference 8.

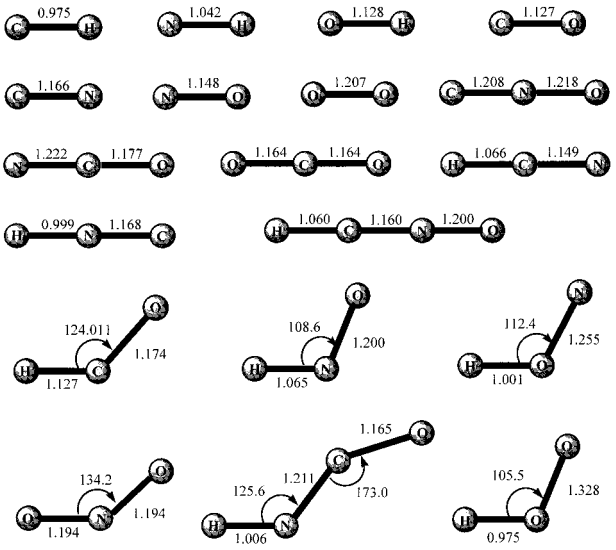

Figure 1. B3LYP/6-311G(d,p) optimized geometries for reactant and products. Bond lengths are in angstroms and angles in degrees.

frequencies of the reactant, products, local minima, and transition states structures are obtained at B3LYP/6-311G(d,p) theory level. Moreover, single-point calculations are performed at CCSD(T)/6-311G(d,p) theory level using the B3LYP/6-311G-(d,p) optimized geometries. The zero-point vibration energy (ZPVE) at the B3LYP/6-311G(d,p) level is also included. To confirm whether the obtained transition states connect with the right reactants and products, the intrinsic reaction coordinate (IRC) calculations are performed at the B3LYP/6-311G(d,p) level.

3. Results and Discussions

3.1. Products. Starting from the reactant **R** CH + NO_2, 11 energetically accessible primary product channels of the title reaction are considered in this paper. These products include **P_1** HCO + NO, **P_2** HNO + CO, **P_3** HON + CO, **P_4** ^{1}NH + CO_2, **P_5** HNCO+^{1}O, **P_6** HCNO+^{1}O, **P_7** HCN+$^1O_2$, **P_8** NCO + OH, **P_9** CNO + OH, **P_{10}** CN + HO_2, and **P_{11}** HNC+$^1O_2$. The secondary product H + CO + NO that was identified experimentally by Rim and Hershberger is also included, namely, **P_{12}**. Figure 1 shows the optimized geometries of the reactant and product molecules and radicals. In Table 1, total and relative energies including ZPVE of all the 12 products as well as the corresponding experimental values of reaction heats are listed. Note that the energy of reactant **R** is set zero for reference. The energetic order of the singlet products at the CCSD(T)/6-311G(d,p)//B3LYP/6-311G(d,p) +ZPVE level is **P_2** (−152.5) > **P_1** (−119.7) > **P_4** (−114.1) > **P_{12}** (−110.9) > **P_8** (−109.8) > **P_3** (−109.3) > **P_7** (−88.5) > **P_{11}** (−73.6) > **P_5** (−67.7) > **P_9** (−47.4) > **P_{10}** (−40.3) > **P_6** (2.2). We can easily find that all these products lie well below the reactant except that **P_6** HCNO+^{1}O is 2.2 kcal/mol higher than **R**. Among the former six low-lying products, the formation of **P_2** HNO + CO, **P_1** HCO + NO, and **P_{12}** H + CO + NO was indicated in the experiment by Rim and Hershberger.[6] Note that the energies of triplet products **P_4'** ^{3}NH + CO_2, **P_5'** HNCO+^{3}O, **P_6'** HCNO+^{3}O, and **P_7'** HCN+$^3O_2$ are also listed for comparison. Clearly, all the singlet products **P_4**, **P_5**, **P_6**, **P_7**, and **P_{11}** are energetically much higher than the corresponding triplet products **P_4'**, **P_5'**, **P_6'**, **P_7'**, and **P_{11}'** since the ground state of NH, O, and O_2 is triplet. It is also worthy of mentioning that product **P_3** HON + CO was ignored in previous papers,[5,6] yet as will be discussed in section 3.4, this product channel at least plays a comparable role to product **P_2** = HNO + CO in determining the final yields.

It is worthwhile to compare our calculated relative energies with the experimentally determined reaction heats of the products.[8] As shown in Table 1, for most products, the theoretical and experimental values agree well, except for **P_4'** ^{3}NH + CO_2 and **P_{12}** H + CO + NO with large discrepancies of 7.0 and 8.1 kcal/mol, respectively. However, as will be shown in section 3.4, such discrepancies will not affect our discussions on the reaction mechanism.

3.2. Isomers. Twenty-five singlet $CHNO_2$ isomers are located as minima with their structures depicted in Figure 2. Table 2 shows the total and relative energies with inclusion of zero-point vibration energies of all the isomers. The vibration frequencies and infrared intensities for the $CHNO_2$ isomers are also listed in Table 4. These isomers can be classified into five groups, i.e., branched chainlike (isomers **1**, **2**, **2′**, **3**, **4**, **4′**, **5**, and **6**), chainlike (isomers **7**, **8**, **8′**, **9**, **10**, and **11**), three-membered ring (isomers **12**, **13**, and **14**) and four-membered ring (isomers **15**, **16**, **17**, **18**, and **19**) and weakly bound complexes (isomers **20**, **21**, and **22**). Note that the isomers **2** and **2′**, **4** and **4′**, and **8** and **8′** are three sets of *cis*−*trans* species. As listed in Table 2, all these isomers are lower in energy than

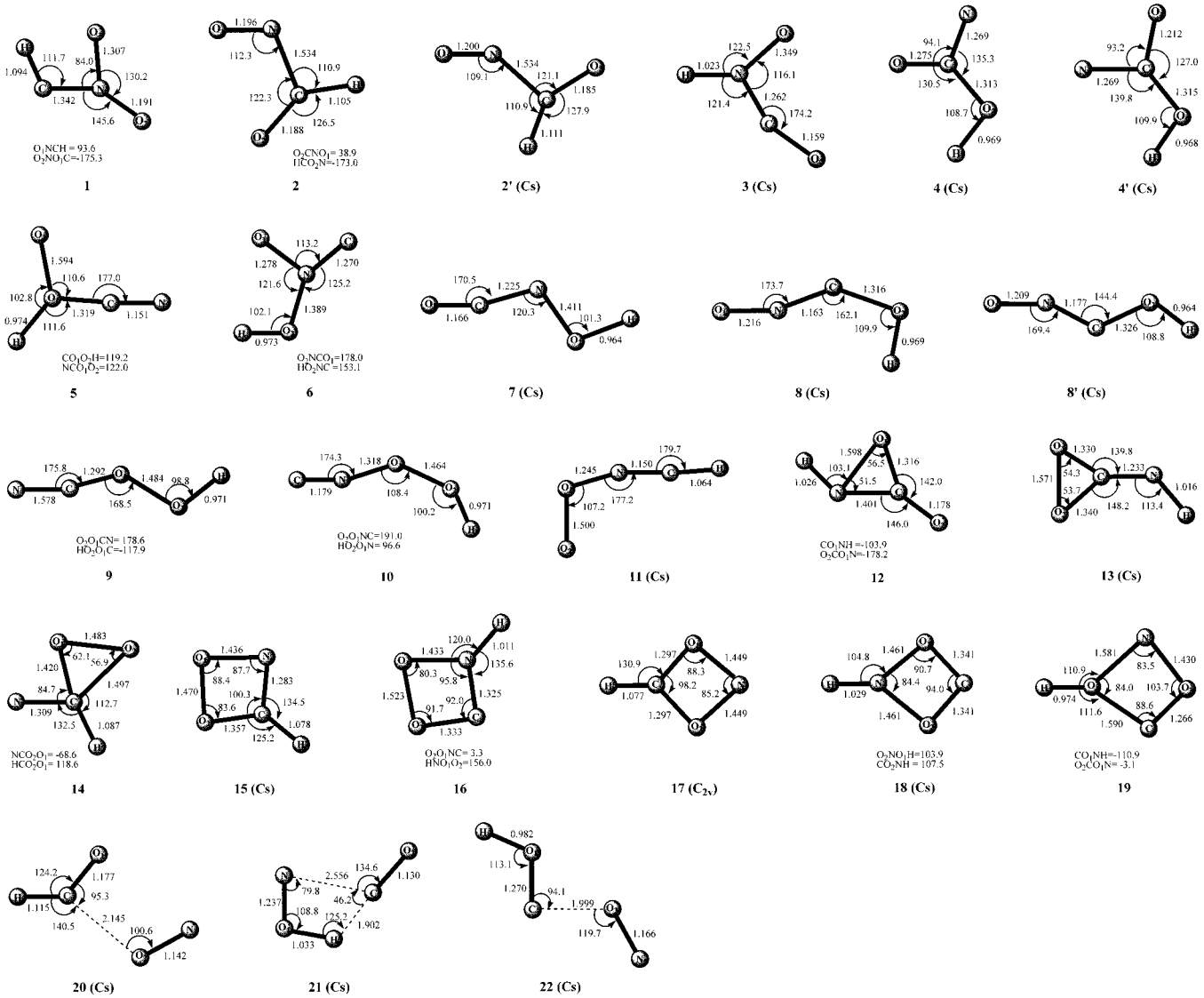

Figure 2. B3LYP/6-311G(d,p) optimized geometries for $CHNO_2$ isomers. Bond lengths are in angstroms and angles in degrees.

TABLE 2: Total (au) and Relative Energies in Parentheses (kcal/mol) as Well as Those Including Zero-Point Vibration Energies (kcal/mol) of the Isomers for the CH + NO_2 Reaction

species	B3LYP/6-311G(d,p)	CCSD(T)/6-311G(d,p)	CCSD(T)/6-311G(d,p) +ZPVE
1	−243.732 590 6 (−67.7)	−243.162 301 6 (−62.6)	−57.3
2	−243.852 675 8 (−143.1)	−243.294 792 5 (−145.7)	−140.2
2'	−243.857 582 1 (−146.1)	−243.299 889 7 (−148.9)	−143.2
3	−243.833 058 4 (−130.8)	−243.256 761 4 (−121.9)	−115.9
4	−243.847 980 2 (−140.1)	−243.287 406 2 (−141.1)	−134.5
4'	−243.846 971 8 (−139.5)	−243.287 062 7 (−140.9)	−136.9
5	−243.722 714 9 (−61.5)	−243.160 070 2 (−61.2)	−55.5
6	−243.713 002 7 (−55.4)	−243.147 888 1 (−53.5)	−48.5
7	−243.894 274 9 (−169.2)	−243.324 978 0 (−164.7)	−157.7
8	−243.837 231 4 (−133.3)	−243.264 037 0 (−126.4)	−120.5
8'	−243.841 298 2 (−135.9)	−243.269 772 9 (−130.0)	−123.4
9	−243.825 221 0 (−125.8)	−243.262 363 3 (−125.4)	−119.3
10	−243.740 412 1 (−72.6)	−243.177 531 2 (−72.1)	−66.9
11	−243.679 297 7 (−34.3)	−243.103 242 0 (−25.2)	−21.2
12	−243.876 172 9 (−157.8)	−243.313 982 8 (−157.8)	−150.7
13	−243.825 778 5 (−126.2)	−243.263 352 6 (−126.0)	−119.5
14	−243.672 079 1 (−29.7)	−243.108 634 7 (−28.9)	−24.2
15	−243.777 986 7 (−96.2)	−243.215 605 5 (−96.0)	−89.1
16	−243.727 748 1 (−64.7)	−243.163 939 9 (−63.0)	−57.1
17	−243.780 980 6 (−98.1)	−243.217 821 3 (−97.4)	−91.0
18	−243.764 681 3 (−87.8)	−243.206 013 8 (−90.0)	−83.0
19	−243.685 268 8 (−38.0)	−243.122 300 3 (−37.5)	−32.8
20	−243.802 295 5 (−100.2)	−243.246 670 3 (−115.5)	−109.6
21	−243.801 979 5 (−111.2)	−243.246 335 5 (−115.3)	−111.3
22	−243.717 253 4 (−58.1)	−243.163 464 2 (−63.3)	−59.5

TABLE 3: Total (a.u.) and Relative Energies in Parentheses (kcal/mol) as Well as Those Including Zero-Point Vibration Energies (kcal/mol) of the Transition States for the CH + NO_2 Reaction

species	B3LYP/6-311G(d,p)	CCSD(T)/6-311G(d,p)	CCSD(T)/6-311G(d,p) +ZPVE
TS1/1	−243.727 193 6 (−64.3)	−243.155 543 0 (−58.3)	−53.5
TS1/2	−243.731 852 3 (−67.2)	−243.161 350 1 (−62.0)	−57.1
TS2/2	−243.852 474 2 (−142.9)	−243.294 743 8 (−145.7)	−140.3
TS2/2'	−243.851 986 9 (−142.6)	−243.293 820 1 (−145.1)	−139.9
TS2/15	−243.749 967 6 (−78.6)	−243.192 358 4 (−81.4)	−76.0
TS2/P_2	−243.779 950 5 (−97.4)	−243.219 666 9 (−98.6)	−94.5
TS2'/3	−243.792 092 8 (−105.0)	−243.220 057 9 (−98.8)	−96.5
TS2'/8'	−243.753 566 5 (−80.9)	−243.178 931 0 (−73.0)	−70.4
TS2'/21	−243.799 750 7 (−109.9)	−243.238 894 7 (−110.6)	−108.6
TS2'/P_1	−243.762 744 0 (−86.6)	−243.249 859 1 (−117.5)	−115.2
TS2'/P_2	−243.793 221 5 (−105.8)	−243.235 464 7 (−108.5)	−107.3
TS3/7	−243.792 513 5 (−105.3)	−243.216 533 9 (−96.6)	−93.0
TS3/12	−243.828 203 7 (−127.7)	−243.252 989 2 (−119.5)	−114.0
TS3/16	−243.725 815 6 (−63.5)	−243.160 813 2 (−61.7)	−56.5
TS3/P_2	−243.828 247 6 (−127.7)	−243.263 828 5 (−126.3)	−121.2
TS4/4	−243.775 702 6 (−94.8)	−243.209 609 6 (−92.3)	−89.4
TS4/4'	−243.837 879 8 (−133.8)	−243.279 382 9 (−136.1)	−120.4
TS4/7	−243.829 113 5 (−128.3)	−243.260 939 9 (−124.5)	−119.1
TS4/8'	−243.773 769 6 (−93.5)	−243.211 888 1 (−93.7)	−88.5
TS5/9	−243.709 415 8 (−53.2)	−243.146 010 3 (−52.4)	−47.1
TS5/10	−243.655 080 4 (−19.1)	−243.091 293 9 (−18.0)	−13.0
TS6/6	−243.712 942 3 (−55.4)	−243.147 827 6 (−53.5)	−48.6
TS6/6*	−243.707 904 0 (−52.2)	−243.143 248 6 (−50.6)	−45.8
TS6/P_3	−243.703 316 5 (−49.3)	−243.140 282 6 (−48.8)	−44.0
TS7/7	−243.884 560 3 (−163.1)	−243.315 304 2 (−158.6)	−125.2
TS7/12	−243.801 012 7 (−110.6)	−243.238 842 6 (−110.6)	−107.3
TS7/P_3	−243.791 869 4 (−104.9)	−243.236 730 2 (−109.3)	−105.8
TS8'/8'	−243.765 898 4 (−88.6)	−243.210 789 2 (−93.0)	−87.7
TS9/9	−243.824 637 4 (−125.5)	−243.261 300 5 (−124.7)	−118.9
TS9/9*	−243.817 986 9 (−121.3)	−243.254 351 9 (−120.3)	−114.5
TS9/10	−243.698 221 2 (−46.1)	−243.135 170 3 (−45.6)	−41.5
TS10/10	−243.732 399 7 (−67.6)	−243.168 787 5 (−66.7)	−61.9
TS10/15	−243.646 062 3 (−13.4)	−243.082 643 2 (−12.6)	−10.0
TS11/11	−243.647 259 0 (−14.2)	−243.076 742 4 (−8.9)	−4.9
TS11/15	−243.668 086 5 (−27.2)	−243.107 841 5 (−28.4)	−24.2
TS11/P_7	−243.677 113 6 (−32.9)	−243.110 509 4 (−30.1)	−27.1
TS12/12	−243.841 878 3 (−136.3)	−243.274 042 5 (−132.7)	−127.1
TS13/13	−243.801 902 0 (−111.2)	−243.234 977 9 (−108.2)	−103.3
TS13/16	−243.699 407 9 (−46.9)	−243.134 235 3 (−45.0)	−40.2
TS13/P_{11}	−243.711 173 3 (−54.3)	−243.140 499 7 (−48.9)	−46.2
TS14/P_7	−243.671 823 2 (−29.6)	−243.107 569 9 (−28.2)	−23.9
TS15/16	−243.673 902 5 (−30.9)	−243.111 876 5 (−30.9)	−27.4
TS17/19	−243.657 904 5 (−20.8)	−243.098 761 3 (−22.7)	−20.1
TS17/P_1	−243.710 001 0 (−53.5)	−243.148 765 3 (−54.1)	−50.0
TS18/P_4	−243.739 084 0 (−71.8)	−243.185 629 5 (−77.2)	−72.4
TSP$_1$/ P$_1$	−243.780 144 8 (−97.6)	−243.231 792 3 (−106.2)	−103.0
TSP$_1$/P$_2$	−243.790 456 1 (−104.0)	−234.231 193 1 (−105.8)	−102.3
TSP$_1$/P$_{12}$	−243.774 002 9 (−93.7)	−243.227 097 6 (−103.2)	−106.3
TSP$_2$/P$_4$	−243.787 567 5 (−102.2)	−243.228 696 9 (−104.2)	−99.6
TSP$_3$/P$_3$	−243.745 015 5 (−75.5)	−243.188 756 2 (−79.2)	−74.6

reactant **R**. At the CCSD(T)/6-311G(d,p)//B3LYP/6-311G-(d,p)+ZPVE level, the energetic order of these isomers can be written as **7** (−157.7) > **12** (−150.7) > **2′** (−143.2) > **2** (−140.2) > **4′** (−136.9) > **4** (−134.5) > **8′** (−123.4) > **8** (−120.5) > **13** (−119.5) > **9** (−119.3) > **3** (−115.9) > **21** (−111.3) > **20** (−109.6) > **17** (−91.0) > **15** (−89.1) > **18** (−83.0) > **10** (−66.9) > **22** (−59.5) > **1** (−57.3) > **16** (−57.1) > **5** (−55.5) > **6** (−48.5) > **19** (−32.8) >**14** (−24.2) > **11** (−21.2). The lowest-lying isomer is the chainlike structure **7** bearing HO−N═C═O skeleton. The second lowest lying isomer **12** is a three-membered species formed by the side attack of ^{1}NH at CO_2. In isomer **12**, both N and C are triple-coordinated while O is double-coordinated. The *cis*−*trans* isomers **2** and **2′** have the branched chainlike structure O═C(H)-N═O. The *cis*−*trans* isomers **4** and **4′**, **8** and **8′** can be viewed as the respective adducts of OH on NCO and CNO radicals both at the C atom site. For simplicity, the structural details of the other isomers are omitted.

In Rim and Hershberger's experiment,[6] a chainlike isomer HCONO was suggested as a very important intermediate to form the observed products HCO + NO, H + CO + NO. However, despite numerous attempts, optimization of such a structure often leads to product $\mathbf{P_1}$ HCO + NO. Also, attempts to search for the respective *cis*- [dihedral angle $\angle HNCO_{(2)} = 0°$] and *trans*-[dihedral angle $\angle HO_{(2)}NC = 0°$] forms of the branched chainlike isomers **3** $O_{(1)}N(H)CO_{(2)}$ and **6** $HO_{(2)}N(C)O_{(1)}$ fail. Moreover, for the chainlike isomers **7**, **8** (**8′**), **9**, **10**, and **11**, searching for several other kinds of isomeric forms is unsuccessful. We take the skeleton $HO_{(2)}NCO_{(1)}$ for example. We can formally write four isomers, isomer with $\angle HO_{(2)}NC = 0°$ and $\angle O_{(2)}NCO_{(1)} = 0°$, isomer with $\angle HO_{(2)}NC = 0°$ and $\angle O_{(2)}NCO_{(1)} = 180°$, isomer with $\angle HO_{(2)}NC = 180°$ and $\angle O_{(2)}NCO_{(1)} = 0°$, and isomer with $\angle HO_{(2)}NC = 180°$ and $\angle O_{(2)}NCO_{(1)} = 180°$. However, only isomer **7** with $\angle HO_{(2)}NC = 180°$ and $\angle O_{(2)}NCO_{(1)} = 180°$ is located.

3.3. Transition States and Isomerization. To make clear the interrelation between various $HCNO_2$ isomers, 50 transition states are obtained. The symbol **TSm/n** is used to denote the transition state connecting the isomers **m** and **n**. The optimized structures of the transition states are given in Figure 3, while the energetics is listed in Table 3. Their vibration frequencies and infrared intensities are presented in Table 5. By means of the transition states and their connected isomers or products, a

TABLE 4: Harmonic Vibration Frequencies (cm^{-1}) with Infrared Intensities in Parentheses (km/mol) for $CHNO_2$ Isomers at the B3LYP/6-311G(d,p) Level

isomers	harmonic frequencies (infrared intensities)
1	254(3) 522(19) 567(21) 854(208) 972(51) 1095(26) 1209(83) 1774(364) 3093(0)
2	88(12) 330(9) 609(3) 702(23) 1000(34) 1333(1) 1673(56) 1836(145) 2965(81)
2'	111(12) 395(22) 514(1) 910(3) 949(9) 1307(6) 1659(47) 1875(167) 2908(75)
3	213(27) 252(14) 569(63) 597(3) 955(50) 1179(86) 1438(18) 2284(478) 3376(26)
4	412(135) 420(13) 499(24) 641(32) 1021(51) 1170(90) 1470(147) 1823(261) 2769(117)
4'	433115) 433(22) 508(8) 644(40) 1014(39) 1172(137) 1484(35) 1798(321) 3782(107)
5	193(12) 400(24) 451(6) 542(76) 685(41) 1027(31) 1220(85) 2392(46) 3696(226)
6	247(18) 299(108) 383(0) 517(22) 944(18) 1249(412) 1468(182) 2345(158) 3810(173)
7	240(8) 253(147) 527(12) 697(21) 886(54) 1297(80) 1501(41) 1305(664) 3825(99)
8	40(47) 107(63) 388(15) 470(12) 900(13) 1257(102) 1424(370) 2475(89) 3715(76)
8'	247(18) 299(108) 383(0) 517(22) 944(18) 1249(412) 1468(182) 2345(158) 3810(173)
9	185(122) 250(14) 509(13) 607(5) 818(5) 1071(8) 1380(14) 2323(42) 3742(81)
10	159(0) 248(73) 344(56) 543(8) 819(15) 943(4) 1381(50) 2140(79) 3725(57)
11	157(74) 222(8) 431(12) 522(3) 617(10) 647(40) 1057(44) 2279(182) 3478(344)
12	554(9) 576(35) 664(15) 939(96) 1075(42) 1127(54) 1240(27) 2046(545) 3403(12)
13	510(24) 600(10) 690(14) 764(92) 883(57) 1083(83) 1154(53) 1978(417) 3556(39)
14	282(33) 408(28) 549(20) 784(4) 959(44) 1122(24) 1230(3) 1424(29) 3153(13)
15	619(15) 796(19) 821(21) 848(7) 1065(11) 1114(44) 1287(31) 1650(15) 3268(1)
16	226(145) 527(84) 589(18) 884(11) 1059(13) 1144(27) 1217(5) 1465(25) 3629(81)
17	533(52) 664(5) 703(4) 779(67) 1117(6) 1156(14) 1376(0) 1493(48) 3284(13)
18	525(10) 779(1) 888(19) 1062(0) 1097(78) 1238(64) 1250(23) 1313(9) 3367(6)
19	325(83) 491(22) 624(89) 711(24) 769(32) 913(8) 966(75) 1407(21) 3713(155)
20	190(19) 279(3) 249(17) 605(21) 633(2) 1086(252) 1793(756) 1961(43) 2806(146)
21	125(13) 136(0) 198(6) 446(80) 791(77) 1372(121) 1519(26) 2182(252) 2674(95)
22	53(5) 197(3) 215(26) 554(92) 615(21) 1154(130) 1394(258) 1722(463) 3409(22)

TABLE 5: Harmonic Vibration Frequencies (cm^{-1}) with Infrared Intensities in Parentheses (km/mol) for $CHNO_2$ Transition States at the B3LYP/6-311G(d,p) Level

species	harmonic frequencies (infrared intensities)
TS1/1	−258(2) 595(45) 622(19) 655(28) 990(26) 1105(14) 1442(54) 1548(258) 3024(1)
TS1/2	−325(115) 504(19) 561(4) 738(220) 973(71) 1023(46) 1193(29) 1882(417) 3178(10)
TS2/2	−71(15) 314(6) 593(3) 833(3) 865(57) 1324(2) 1688(66) 1864(117) 2973(57)
TS2/2'	−127(6) 296(5) 471(24) 707(33) 1045(5) 1338(5) 1659(50) 1837(183) 2927(74)
TS2/15	−1165(110) 591(25) 860(11) 939(25) 1038(80) 1111(8) 1286(11) 1410(17) 3213(0)
TS2/P_2	−1241(410) 226(872) 270(0) 475(30) 592(5) 852(24) 1744(872) 1952(118) 3534(104)
TS2'/3	−1293(307) 297(19) 414(50) 546(22) 718(1) 1088(28) 1498(349) 1714(70) 1952(311)
TS2'/8'	−1631(1061) 233(9) 305(12) 309(7) 534(1) 939(16) 1404(506) 2122(71) 2628(237)
TS2'/21	−773(51) 130(1) 134(3) 630(55) 744(36) 1060(30) 1400(250) 1789(37) 2139(420)
TS2'/P_1	−225(5) 52(3) 170(1) 312(0) 381(36) 1082(591) 1742(600) 1980(984) 2564(356)
TS2'/P_2	−903(160) 92(1) 170(2) 418(43) 496(14) 1027(115) 1482(179) 1867(975) 1994(150)
TS3/7	−1297(746) 139(11) 405(82) 539(58) 607(15) 797(15) 1251(1) 2288(711) 2969(347)
TS3/12	−399(70) 351(176) 418(29) 541(10) 902(26) 1161(74) 1317(1) 2328(637) 3503(70)
TS3/16	−302(238) 138(113) 528(29) 852(21) 992(9) 1240(40) 1364(75) 1573(35) 3652(91)
TS3/P_2	−437(53) 140(7) 464(50) 613(6) 993(125) 1388(229) 1504(23) 2009(301) 3010(31)
TS4/4	−1995(286) 257(2) 579(1) 707(8) 970(108) 1111(27) 1422(187) 1539(63) 2102(161)
TS4/4'	−451(137) 386(17) 519(2) 591(39) 991(69) 1179(130) 1400(73) 1787(216) 3811(145)
TS4/7	−384(23) 340(91) 516(11) 669(28) 918(87) 1158(91) 1375(30) 1688(94) 3757(139)
TS4/8'	−538(37) 322(25) 429(81) 618(110) 943(240) 1180(21) 1289(207) 1698(41) 3788(168)
TS5/9	−457(127) 404(13) 422(7) 725(16) 857(58) 975(44) 1125(113) 2246(137) 3630(159)
TS5/10	−386(144) 395(29) 641(5) 758(2) 829(106) 957(5) 1164(67) 1738(45) 3648(166)
TS6/6	−107(142) 288(19) 479(16) 542(3) 832(121) 1162(61) 1340(144) 1724(1) 3694(113)
TS6/6*	−46(122) 263(31) 493(6) 537(6) 799(90) 1184(146) 1373(16) 1660(30) 3705(65)
TS6/P_3	−442(1) 334(73) 390(50) 439(34) 899(49) 1020(52) 1391(101) 1797(36) 3720(99)
TS7/7	−216(94) 223(38) 515(35) 696(23) 861(43) 1388(10) 1391(18) 2301(603) 3743(24)
TS7/12	−1670(75) 436(40) 598(59) 624(11) 776(81) 908(107) 1125(6) 2049(594) 2439(71)
TS7/P_3	−102(1) 54(11) 146(14) 256(6) 527(159) 1249(86) 1461(9) 2193(171) 3216(67)
TS8'/8'	−283(0) 366(3) 481(5) 724(46) 779(43) 1245(115) 1393(97) 1670(65) 3728(132)
TS9/9	−144(146) 241(0) 499(7) 601(6) 814(6) 1074(11) 1242(70) 2324(41) 3758(99)
TS9/9*	−341(115) 235(19) 499(21) 626(1) 802(9) 1096(30) 1423(46) 2304(50) 3693(39)
TS9/10	−448(11) 257(2) 376(14) 425(105) 567(58) 933(64) 1428(51) 1833(13) 3704(16)
TS10/10	−410(124) 172(4) 298(4) 522(16) 814(26) 960(19) 1420(45) 2119(59) 3719(40)
TS10/15	−1488(131) 409(106) 559(5) 725(53) 880(6) 981(88) 1142(15) 1509(26) 2233(94)
TS11/11	−479(294) 396(0) 462(33) 719(132) 765(30) 815(10) 1009(18) 1995(269) 3254(39)
TS11/15	−417(10) 479(70) 672(321) 743(37) 815(33) 926(17) 1099(16) 1627(32) 3187(12)
TS11/P_7	−545(73) 171(9) 383(188) 575(326) 699(78) 755(32) 1066(40) 1834(55) 3249(42)
TS12/12	−948(251) 476(58) 600(10) 650(11) 772(104) 1050(28) 1191(10) 2080(699) 3729(282)
TS13/13	−853(271) 243(170) 546(2) 615(1) 710(25) 819(43) 1103(45) 2129(621) 3940(471)
TS13/16	−456(159) 424(27) 601(105) 621(13) 878(7) 943(89) 1360(40) 1633(100) 3543(104)
TS13/P_{11}	−562(64) 99(31) 256(156) 260(140) 338(66) 511(6) 1208(145) 2063(228) 3813(506)
TS14/P_7	−314(56) 352(10) 537(19) 822(16) 976(25) 1094(30) 1210(4) 1476(27) 3180(7)
TS15/16	−1459(59) 633(2) 721(47) 828(5) 1063(7) 1133(64) 1163(11) 1335(47) 2188(48)
TS17/19	−1495(116) 386(58) 677(5) 869(42) 934(19) 1050(4) 1221(10) 1314(42) 2018(21)
TS17/P_1	−694(53) 431(56) 631(30) 854(29) 895(19) 999(55) 1310(44) 1464(71) 2946(40)
TS18/P_4	−391(124) 268(61) 531(8) 680(22) 905(27) 1219(49) 1345(60) 1713(237) 2228(7)
TSP_1/P_1	−303(4) 164(4) 270(7) 411(10) 656(13) 1148(395) 1705(531) 1939(608) 2599(165)
TSP_1/P_2	−250(10) 135 (9) 310(57) 349(4) 768(12) 1124(207) 1687(637) 1936(240) 2763(183)
TSP_2/P_4	−523(147) 114(8) 455(73) 580(13) 770(78) 1081(66) 1536(34) 1963(364) 3351(6)
TSP_3/P_3	−392(140) 414(4) 483(4) 688(4) 751(73) 915(38) 1318(68) 1516(54) 3754(82)

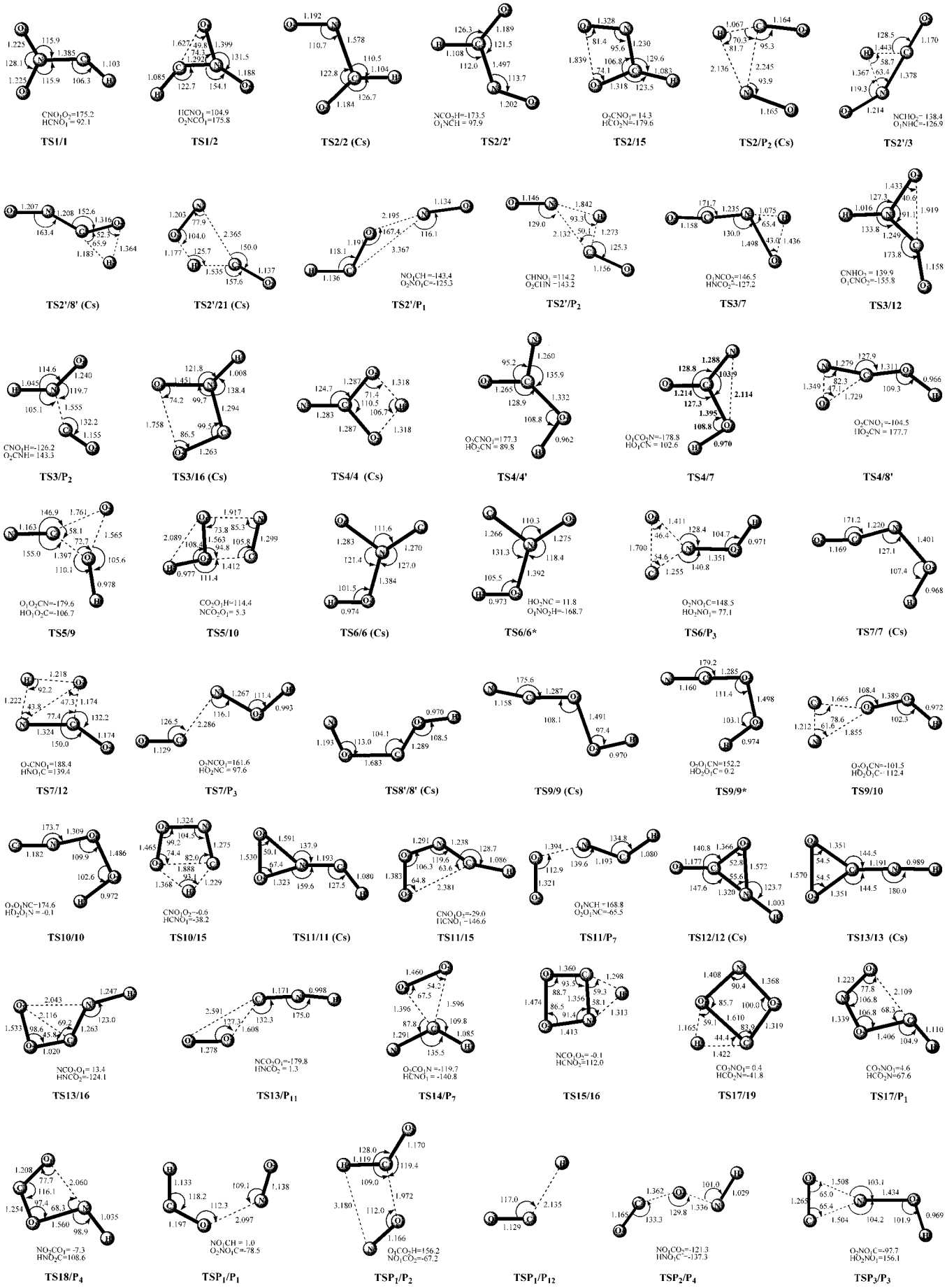

Figure 3. B3LYP/6-311G(d,p) optimized geometries for $CHNO_2$ transition states. Bond lengths are in angstroms and angles in degrees.

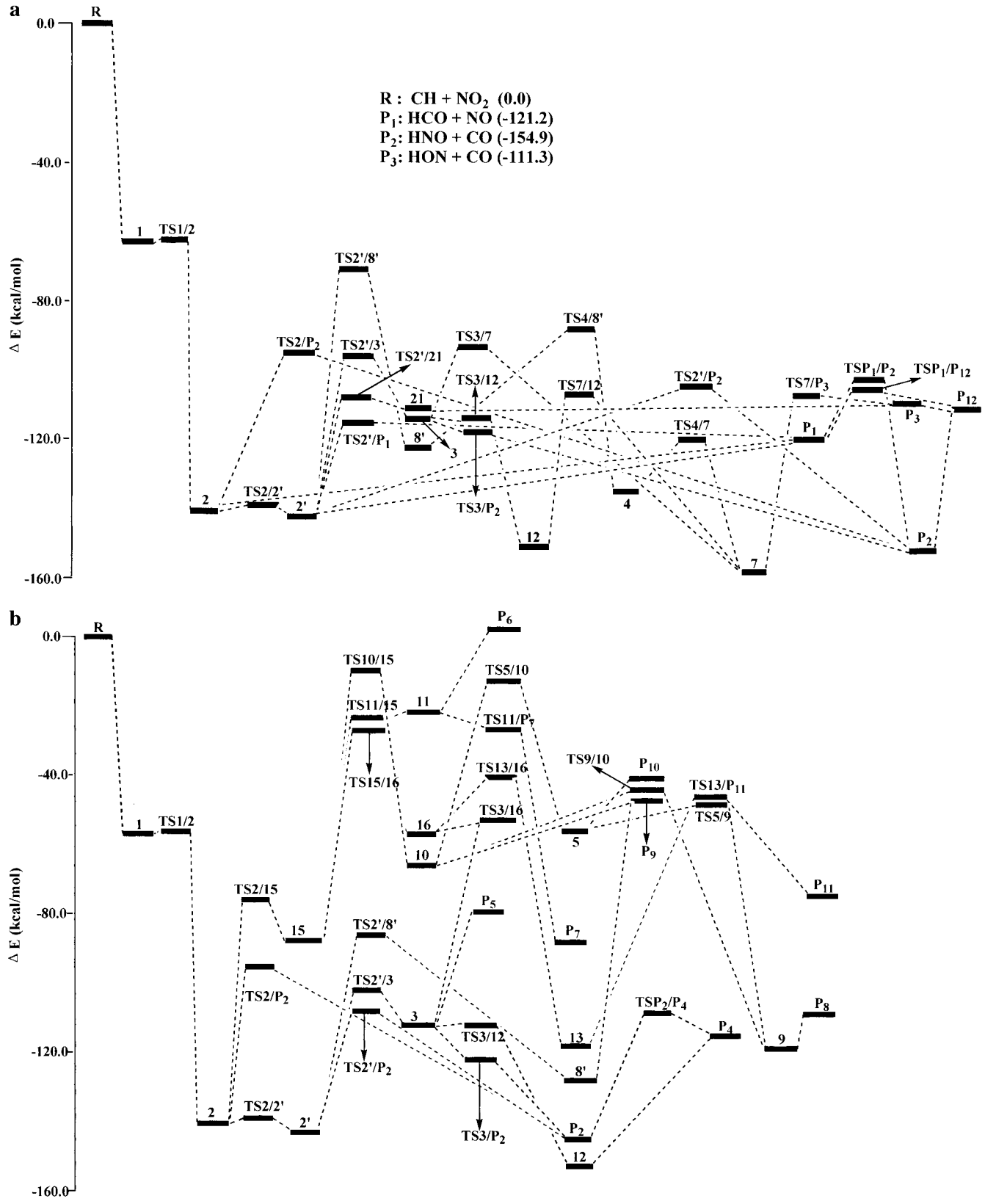

Figure 4. (a) Schematic pathways for the products $\mathbf{P_1}$ HCO + NO, $\mathbf{P_2}$ HNO + CO, $\mathbf{P_3}$ HON + CO and $\mathbf{P_{12}}$ H + CO + NO for the CH + NO_2 reaction. Relative energies are calculated at the CCSD(T)/6-311G(d,p)//B3LYP/6-311G(d,p)+ZPVE level. (b) Schematic pathways for the products $\mathbf{P_4}$ ^{1}NH + CO_2, $\mathbf{P_5}$ HNCO+^{1}O, $\mathbf{P_6}$ HCNO+^{1}O, $\mathbf{P_7}$ HCN+$^1O_2$, $\mathbf{P_8}$ NCO + OH, $\mathbf{P_9}$ CNO + OH, $\mathbf{P_{10}}$ CN + HO_2, and $\mathbf{P_{11}}$ HNC+$^1O_2$ for the CH + NO_2 reaction. Relative energies are calculated at the CCSD(T)/6-311G(d,p)//B3LYP/6-311G(d,p)+ZPVE level.

schematic potential energy surface (PES) of $HCNO_2$ in singlet is plotted in Figure 4a,b. Among these transition states, fifteen species (**TS1/1**, **TS2/2**, **TS4/4**, **TS6/6**, **TS6/6***, **TS7/7**, **TS8′/8′**, **TS9/9**, **TS9/9***, **TS10/10**, **TS11/11**, **TS12/12**, **TS13/13**, **TSP$_1$/P$_1$**, and **TSP$_3$/P$_3$**) are associated with the degenerate isomerization between isomers or products. Since they are unimportant for discussing the mechanism of the title reaction, their details are not given and are not presented in Figure 4a,b, either.

On the basis of the PES, we can discuss the isomerization and dissociation processes of various singlet $HCNO_2$ isomers starting from reactant **R**. The initial step is formation of isomer $HCNO_2$ (**1**) when the C atom of CH attacks the NO π bonding of NO_2. Isomer **1** can easily isomerize to the low-lying isomer *cis*-OC(H)NO **2** and then to *trans*-OC(H)NO **2′** with the respective barrier of only 0.2 and 0.3 kcal/mol. The formation of product $\mathbf{P_1}$ HCO + NO may take place via two pathways: **Path P_1 (1)**: **R → 1 → 2 → P_1** and **Path P_1 (2)**: **R → 1 → 2 → 2′ → P_1**. Since the interconversion between **2** and **2′** is very easy (the barrier from **2′** to **2** is just 3.0 kcal/mol), both pathways may be significant in determining the formation of $\mathbf{P_1}$. It should be pointed out that we find no dissociation transition states of **2** and **2′** to $\mathbf{P_1}$ at the C atom site. Surprisingly, we happen to find a transition state **TS2′/P_1**, whose structure is very loose and a little strange, i.e., the distance between N and O atoms (2.195 Å) is much longer than that between N and C atoms (3.367 Å). This may, on the other hand, mean that the NO attack on HCO radical at the C atom site is barrierless while attack at the O atom site needs to overcome the barrier of 4.5 kcal/mol. It should be noted that for **TS2′/P_1**, the relative energy calculated at the B3LYP level (−86.6 kcal/mol) differs considerably from the CCSD(T) value (−115.2 kcal/mol) by about 30 kcal/mol. This indicates that electron correlation is rather important in determining the energetics of such a process. Further calculations at higher-levels such as configuration interaction method may surely be useful. However, we expect that NO attack at the O atom of HCO to form isomer OC(H)-NO **2′** is a barrier-consumed process due to the repulsion between the lone-pair electrons at O atom of HCO and at N atom of NO. Then it is safe for us to conclude that the direct dissociation of isomer **2** and **2′** to $\mathbf{P_1}$ is more favorable than that via **TS2′/P_1**, and the significant electron correlation effect on **TS2′/P_1** will not influence the discussion of reaction mechanism. Therefore, **TS2′/P_1** will not be considered further in the present paper.

Product $\mathbf{P_2}$ HNO + CO may be formed via five reaction pathways:

Path P_2 (1): **R → 1 → 2 → P_2**

Path P_2 (2): **R → 1 → 2 → 2′ → P2**

Path P_2 (3): **R → 1 → 2 → 2′ → 3 → P_2**

Path P_2 (4): **R → 1 → 2 → 2′ → 8′ → 4 → 7 → 3 → P_2**

Path P_2 (5): **R → 1 → 2 → 2′ → 8′ → 4 → 7 → 12 → 3 → P_2**

In principle, all the five pathways may contribute to the formation of $\mathbf{P_2}$ since all the intermediates and transition states are significantly lower in energy than reactant **R**. Yet, since the relative energy of the rate determining transition state **TS2′/P_2** (−107.3 kcal/mol) of **Path P_2 (2)** is much lower than **TS2/P_2** (−94.5 kcal/mol) of **Path P_2 (1)**, **TS2′/3** (−96.5 kcal/mol) of **Path P_2 (3)** and **TS2′/8′** (−70.4 kcal/mol) of both **Path P_2 (4)** and **Path P_2 (5)**, **Path P_2 (2)** may be the most feasible among the five pathways. In addition, **Path P_2 (2)** is relatively very simple. In the present and later discussions, the most feasible pathways are underlined.

For product $\mathbf{P_3}$ HON + NO, there are four energetically accessible pathways:

Path P_3 (1): **R → 1 → 2 → 2′ → 21 → P_3**

Path P_3 (2): **R → 1 → 2 → 2′ → 3 → 7 → P_3**

Path P_3 (3): **R → 1 → 2 → 2′ → 3 → 12 → 7 → P_3**

Path P_3 (4): **R → 1 → 2 → 2′ → 8′ → 4 → 7 → P_3**

The relative energy of the rate determining transition state **TS2′/21** (−108.6 kcal/mol) of **Path P_3 (1)** is much lower than **TS3/7** (−93.0 kcal/mol) of **Path P_3 (2)**, **TS2′/3** (−96.5 kcal/mol) of **Path P_3 (3)** and **TS2′/8′** (−70.4 kcal/mol) of **Path P_3 (4)**. Then, **Path P_3 (1)** may be the most feasible pathway.

There are three pathways to form product $\mathbf{P_4}$ ^{1}NH + CO_2 and product $\mathbf{P_5}$ HNCO+^{1}O each. They include:

Path P_4 (1): **R → 1 → 2 → 2′ → 3 → 12 → P_4**

Path P_4 (2): **R → 1 → 2 → 2′ → 8′ → 4 → 7 → 12 → P_4**

Path P_4 (3): **R → 1 → 2 → 2′ → 8′ → 4 → 7 → 3 → 12 → P_4**

and

Path P_5 (1): **R → 1 → 2 → 2′ → 3 → P_5**

Path P_5 (2): **R → 1 → 2 → 2′ → 8′ → 4 → 7 → 12 → 3 → P_5**

Path P_5 (3): **R → 1 → 2 → 2′ → 8′ → 4 → 7 → 3 → P_5**

Certainly, **Path P_4 (1)** and **Path P_5 (1)** are the respective most feasible pathways to form $\mathbf{P_4}$ and $\mathbf{P_5}$.

For formation of the products $\mathbf{P_6}$ HCNO+^{1}O and $\mathbf{P_7}$ HCN+$^1O_2$, the shared intermediate prior to dissociation is the chainlike isomer HCNOO **11**. It can be reached via four pathways to form both $\mathbf{P_6}$ and $\mathbf{P_7}$:

Path P_6 (1): **R → 1 → 2 → 15 → 11 → P_6**

Path P_6 (2): **R → 1 → 2 → 2′ → 3 → 16 → 15 → 11 → P_6**

Path P_6 (3): **R → 1 → 2 → 2′ → 8′ → 4 → 7 → 3 → 16 → 15 → 11 → P_6**

Path P_6 (4): **R → 1 → 2 → 2′ → 8′ → 4 → 7 → 12 → 3 → 16 → 15 → 11 → P_6**

and

Path P_7 (1): **R → 1 → 2 → 15 → 11 → P_7**

Path P_7 (2): **R → 1 → 2 → 2′ → 3 → 16 → 15 → 11 → P_7**

Path P_7 (3): **R → 1 → 2 → 2′ → 8′ → 4 → 7 → 3 → 16 → 15 → 11 → P_7**

Path P_7 (4): **R → 1 → 2 → 2′ → 8′ → 4 → 7 → 12 → 3 → 16 → 15 → 11 → P_7**

Of course, the simple **Path P_6 (1)** and **Path P_7 (1)** are the most feasible pathways for P_6 and P_7, respectively.

Both the chainlike isomers **HONCO 7** and **HOOCN 9** are the last-step intermediates prior to final dissociation to product P_8 NCO + OH. Then principally the following 11 pathways, i.e.,

Path P_8 (1): **R → 1 → 2 → 2′ → 3 → 7 → P_8**

Path P_8 (2): **R → 1 → 2 → 2′ → 3 → 12 → 7 → P8**

Path P_8 (3): **R → 1 → 2 → 2′ → 8′ → 4 → 7 → P_8**

Path P_8 (4): **R → 1 → 2 → 15 → 10 → 9 → P_8**

Path P_8 (5): **R → 1 → 2 → 2′ → 3 → 16 → 15 → 10 → 9 → P_8**

Path P_8 (6): **R → 1 → 2 → 2′ → 8′ → 4 → 7 → 3 → 16 → 15 → 10 → 9 → P_8**

Path P_8 (7): **R → 1 → 2 → 2′ → 8′ → 4 → 7 → 12 → 3 → 16 → 15 → 10 → 9 → P_8**

Path P_8 (8): **R → 1 → 2 → 15 → 10 → 5 → 9 → P_8**

Path P_8 (9): **R → 1 → 2 → 2′ → 3 → 16 → 15 → 10 → 5 → 9 → P_8**

Path P_8 (10): **R → 1 → 2 → 2′ → 8′ → 4 → 7 → 3 → 16 → 15 → 10 → 5 → 9 → P_8**

Path P_8 (11): **R → 1 → 2 → 2′ → 8′ → 4 → 7 → 12 → 3 → 16 → 15 → 10 → 5 → 9 → P_8**

can lead to P_8. Surely, the energy of the rate determining transition state **TS10/15** (−10.0 kcal/mol) is rather high. Thus, the eight pathways **Path P_8 (4−11)** involving isomers **10** and **15** may contribute much less to the formation of P_8. The rate determining transition states of **Path P_8 (1)**, **Path P_8 (2)** and **Path P_8 (3)** are **TS3/7**, **TS2′/3**, and **TS2′/8′**, respectively. Since **TS3/7** (−93.0 kcal/mol) and **TS2′/3** (−96.5 kcal/mol) lie energetically much lower than **TS2′/8′** (−70.4 kcal/mol), both **Path P_8 (1)** and **Path P_8 (2)** may overwhelm over **Path P_8 (3)** to form P_8. In more detail, starting from isomer **2**, conversion to isomer **12** and then to isomer **7** may be more competitive than direct conversion to isomer **7** since **TS3/7** (−93.0 kcal/mol) lies higher than **TS3/12** (−114.0 kcal/mol) and **TS7/12** (−107.3 kcal/mol). As a result, **Path P_8 (2)** is the most probable pathway to form P_8.

Similarly, considering the structural features, the direct dissociation of both the chainlike isomers HOCNO **8′** and HOONC **10** may produce product P_9 CNO + OH Then we can write 10 energetically accessible pathways as

Path P_9 (1): **R → 1 → 2 → 2′ → 8′ → P_9**

Path P_9 (2): **R → 1 → 2 → 2′ → 3 → 7 → 4 → 8′ → P_9**

Path P_9 (3): **R → 1 → 2 → 2′ → 3 → 12 → 7 → 4 → 8′ → P_9**

Path P_9 (4): **R → 1 → 2 → 15 → 16 → 3 → 2′ → 8′ → P_9**

Path P_9 (5): **R → 1 → 2 → 15 → 16 → 3 → 7 → 4 → 8′ → P_9**

Path P_9 (6): **R → 1 → 2 → 15 → 16 → 3 → 12 → 7 → 4 → 8′ → P_9**

Path P_9 (7): **R → 1 → 2 → 15 → 10 → P_9**

Path P_9 (8): **R → 1 → 2 → 2′ → 3 → 16 → 15 → 10 → P_9**

Path P_9 (9): **R → 1 → 2 → 2′ → 8′ → 4 → 7 → 3 → 16 → 15 → 10 → P_9**

Path P_9 (10): **R → 1 → 2 → 2′ → 8′ → 4 → 7 → 12 → 3 → 16 → 15 → 10 → P_9**

From the relative energies of the transition states involved in these pathways, we can easily find that the rate determining **TS4/8′** (−88.5 kcal/mol) of **Path P_9 (2,3)** lies much lower than **TS2′/8′** (−70.4 kcal/mol) of **Path P_9 (1)**, **TS15/16** (−27.4 kcal/mol) of **Path P_9 (4−6)** and **TS10/15** (−12.6 kcal/mol) of **Path P_9 (7−10)**. Moreover, the second rate determining transition states of **Path P_9 (2)** and **Path P_9 (3)** are **TS3/7** (−93.0 kcal/mol) and **TS7/12** (−107.3 kcal/mol), respectively. While **TS7/12** is 14.3 kcal/mol lower than **TS3/7**, **Path P_9 (3)** is expected to play a predominant role over **Path P_9 (2)** for formation of P_9.

Finally, we can obtain eight pathways for product P_{10} CN + HO_2 and four pathways for product P_{11} HNC+$^1O_2$ as follows:

Path P_{10} (1): **R → 1 → 2 → 15 → 10 → 5 → P_{10}**

Path P_{10} (2): **R → 1 → 2 → 2′ → 3 → 16 → 15 → 10 → 5 → P_{10}**

Path P_{10} (3): **R → 1 → 2 → 2′ → 8′ → 4 → 7 → 3 → 16 → 15 → 10 → 5 → P_{10}**

Path P_{10} (4): **R → 1 → 2 → 2′ → 8′ → 4 → 7 → 12 → 3 → 16 → 15 → 10 → 5 → P_{10}**

Path P_{10} (5): **R → 1 → 2 → 15 → 10 → 9 → 5 → P_{10}**

Path P_{10} (6): **R → 1 → 2 → 2′ → 3 → 16 → 15 → 10 → 9 → 5 → P_{10}**

Path P_{10} (7): **R → 1 → 2 → 2′ → 8′ → 4 → 7 → 3 → 16 → 15 → 10 → 9 → 5 → P_{10}**

Path P_{10} (8): **R → 1 → 2 → 2′ → 8′ → 4 → 7 → 12 → 3 → 16 → 15 → 10 → 9 → 5 → P_{10}**

and

Path P_{11} (1): R → 1 → 2 → 15 → 16 → 13 → P_{11}

Path P_{11} (2): R → 1 → 2 → 2′ → 3 → 16 → 13 → P_{11}

Path P_{11} (3): R → 1 → 2 → 2′ → 8′ → 4 → 7→ 3 → 16 → 13 → P_{11}

Path P_{11} (4): R → 1 → 2 → 2′ → 8′ → 4 → 7 → 12 → 3 → 16 → 13 → P_{11}

For P_{10}, the indirect conversion from isomer **10** to **9** and then **9** to **5** is much easier than direct conversion from **10** to **5**. Then **Path P_{10} (5−8)** are more competitive than **Path P_{10} (1−4)**. Also, **TS3/16** (−56.5 kcal/mol) is considerably higher than **TS2/15** (−76.0 kcal/mol). Then **Path P_{10} (5)** is more competitive than **Path P_{10} (6−8)**. For P_{11}, since the rate determining **TS13/16** (−40.2 kcal/mol) of **Path P_{11} (2−4)** is much lower than **TS15/16** (−27.4 kcal/mol) of **Path P_{11} (1)**, **Path P_{11} (1)** is surely the most unimportant pathway. Moreover, the direct conversion of isomer **2′** to isomer **3** is much more competitive than indirect pathways via isomer **8′** since **TS2′/3** (−96.5 kcal/mol) lies much lower than **TS2′/8′** (−70.4 kcal/mol). Therefore, **Path P_{10} (5)** and **Path P_{11} (2)** are respective most feasible pathways for P_{10} and P_{11}.

It is worthy of note that two inter atom-abstraction transition states between products, namely, **TSP_1/P_2** (H-abstraction from HNO to CO and from HCO to NO) and **TSP_2/P_4** (O-abstraction from HNO to CO and from CO_2 to NH), are also located. Once either of the two products is formed, the separate species need to make reorientation and be well kept together. However, in normal cases, the chance for such secondary intermolecular processes to take place is very rare. Then both intermolecular processes may be unimportant despite that **TSP_1/P_2** (−102.3 kcal/mol) and **TSP_2/P_4** (−99.6 kcal/mol) are close in energy to **TSP_1/P_{12}** (−106.3 kcal/mol) and P_{12} (−110.9 kcal/mol), respectively. Note that **TSP_1/P_{12}** is associated with a intramolecular dissociation within HCO. Therefore, **TSP_1/P_2** and **TSP_2/P_4** are not included in the discussion of the most feasible pathways of the products P_1, P_2 and P_4.

Moreover, no reaction pathways involving the branched chainlike isomer HON(C)O **6** (−48.5 kcal/mol), four-membered ring isomers cOOC(N)H **14** (−24.2 kcal/mol), cONOCH **17** (−91.0 kcal/mol), cOCONH **18** (−83.0 kcal/mol) and cNOCOH **19** (−32.8 kcal/mol), and weakly bound complexes HCO···ON **20** (−109.6 kcal/mol) and HOC···ON **22** (−59.5 kcal/mol) could be found though we obtain some transition states of these possible pathways, i.e., **$TS6/P_3$** (−44.0 kcal/mol), **$TS14/P_7$** (−23.9 kcal/mol), **TS17/19** (−20.1 kcal/mol), **$TS17/P_1$** (−50.0 kcal/mol), and **$TS18/P_4$** (−72.4 kcal/mol). Conversion from reactant **R** to the isomers **6**, **14**, **17**, **18**, and **19** is expected to take complex processes with high barriers. Then, the seven isomers and the five transition states are not given in Figure 4,b, either.

It should be pointed out the barriers for **3→P_2** (−5.3 kcal/mol) **11→15** (−3.0 kcal/mol), and **11→P_7** (−5.9 kcal/mol) show abnormally negative values at the CCSD(T)/6-311G(d,p)//B3LYP/6-311G(d,p)+ZPVE level, though they are positive at the B3LYP/6-311G(d,p) level. This may at least indicate the kinetic instability of the isomers **3** and **11**.

3.4. Mechanism. In section 3.3, we have obtained the most feasible reaction pathways for the 11 primary products. Here, for discussions easier, they are listed again as follows:

Path P_1 (1): R → 1 → 2 → P_1 and
Path P_1 (2): R → 1 → 2 → 2′ → P_1

Path P_2 (2): R → 1 → 2 → 2′ → P_2

Path P_3 (1): R → 1 → 2 → 2′ → 21 → P_3

Path P_4 (1): R → 1 → 2 → 2′ → 3 → 12 → P_4

Path P_5 (1): R → 1 → 2 → 2′ → 3 → P_5

Path P_6 (1): R → 1 → 2 → 15 → 11 → P_6

Path P_7 (1): R → 1 → 2 → 15 → 11 → P_7

Path P_8 (2): R → 1 → 2 → 2′ → 3 → 12 → 7 → P_8

Path P_9 (3): R → 1 → 2 → 2′ → 3 → 12 → 7 → 4 → 8′ → P_9

Path P_{10} (5): R → 1 → 2 → 15 → 10 → 9 → 5 → P_{10}

Path P_{11} (2): R→1→2→2′→3→16→13→P_{11}

By means of these most feasible pathways, let us discuss the possible mechanism of the title reaction.

The products P_5 HNCO+^{1}O (−67.7 kcal/mol), P_6 HCNO+^{1}O (2.2 kcal/mol), P_9 CNO + OH (−47.4 kcal/mol), P_{10} CN + HO_2 (−40.3 kcal/mol), and P_{11} HNC+$^1O_2$ (−73.6 kcal/mol) lie rather high. This thermodynamically prevents their possible experimental existence with detectable yields relative to the low-lying products P_1 HCO + NO (−119.7 kcal/mol), P_2 HNO + CO (−152.5 kcal/mol), P_3 HON + CO (−109.3 kcal/mol), P_{12} H + CO + NO (−110.9 kcal/mol), P_4 ^{1}NH + CO_2 (−114.1 kcal/mol), and P_8 NCO + OH (−109.8 kcal/mol). Additionally, though P_7 HCN+$^1O_2$ (−88.5 kcal/mol) is low-lying, the high-energy **TS11/15** (−24.2 kcal/mol) along its most feasible pathway also makes it unlikely to be observable in experiments.

Let us compare the pathways of the remaining five primary products P_1, P_2, P_3, P_4, and P_8 as well as one secondary product P_{12}, each of which lies more than 100 kcal/mol below reactant **R**. First, **TS3/12** (−114.0 kcal/mol) is higher than **$TS3/P_2$**, and **TS7/12** (−107.3 kcal/mol) is higher than P_4 (−114.1 kcal/mol). Then formation of P_8 via **Path P_8 (1)** may be less likely than P_4 and that of P_4 via **Path P_4 (1)** less likely than that of P_2. Second, we expect that formation of P_1 HCO + NO is much more competitive than that of P_2 HNO + CO and P_3 HON + CO since the relative energy of P_1 (−119.7 kcal/mol) is significantly lower than that of **$TS2'/P_2$** (−107.3 kcal/mol) of **Path P_2 (2)** and **TS2′/21** (−108.6 kcal/mol) of **Path P_3 (1)**. P_2 and P_3 may have comparable abundance when produced. Because of the rather large heat (more than 140 kcal/mol) released from reactant **R** to the isomers **2** and **2′**, further direct dissociation of most of HCO in P_1, HNO in P_2 and HON in P_3 to form the same secondary product P_{12} H + CO + NO may be very facile. Then in the final observed products, the almost exclusive product may be P_{12} H + CO + NO, whereas the remaining P_1 HCO + NO contains a very small amount and the yields of the products P_2 HNO + CO and P_3 HON + CO should be even much smaller. The remaining products, however, may have undetectable yields.

3.5. Comparison with Experiments. Now let us apply our calculated mechanism to discuss the deduced branching ratios of the title reaction in a very recent diode laser study by Rim and Hershberger.[6] They found that CO, CO_2, and NO were detected in significant yield (CO_2 occupies only a small amount), while DCN (from $CDBr_3$), N_2O, HCNO and HNCO in undetectably low yields. Our results that **P₄** ^{1}NH + CO_2 may be negligible compared to **P₁₂** H + CO + NO agree well with Rim and Hershberger[6] that CO_2 was produced mainly via the secondary reaction HCO + NO_2 → H + NO + CO_2. Also, our calculations show that among the total product distributions, **P₁₂** H + CO + NO may be the almost exclusive product and **P₁** HCO + NO may occupy a very small amount with **P₂** HNO + CO and **P₃** HON + NO even much less. This is in excellent agreement with Rim and Hershberger's experimental fact that considerable CO and NO were detected. On the basis of consideration of product yields and secondary chemistry, Rim and Hershberger found that the major product channel is H + CO + NO or HNO + CO (together accounting for 92 ± 4%), whereas HCO + NO is a minor product channel (8 ± 4%). They were not able to distinguish between product **P₂** HNO + CO and.**P₁₂** H + CO + NO because both produce one CO molecule for every CH radical consumed. However, our calculations show that another product **P₃** HON + CO, which was completely ignored by both Wagal[5] and Rim and Hershberger,[6] may partly contribute to the final high abundance of **P₁₂** H + CO + NO in the same role as **P₂** HNO + CO does. In fact, Rim and Hershberger found that the experimental NO yields were inconsistent with their predictions. They ascribed the discrepancy to some possible secondary reactions as Br + NO_2+M → $BrNO_2$+M → BrO + NO+M and CHBr + NO_2→CHOBr + NO. We feel that contribution of the reaction CH + NO_2→HON + CO→H + CO + NO should also be considered. Therefore, Rim and Hershberger's conclusion might be better revised as that the major product channel is H + CO + NO, HNO + CO or HON + CO (together accounting for 92 ± 4%), whereas HCO + NO is a minor product channel (8 ± 4%).

On the basis of the simple transition state theory, we also calculate the relative abundance of the primary products **P₁** HCO + NO, **P₂** HNO + CO and **P₃** HON + NO from the intermediate OC(H)NO **2′** (for simplicity, the three processes are refereed to as reaction 1, 2 and 3, respectively). The rate constant formula $k = KT/h\ e^{\Delta S/R}e^{-\Delta E/RT}$ is used, where k, ΔS, and ΔE denote the rate constants (k_1, k_2, and k_3), entropy differences (ΔS_1, ΔS_2, and ΔS_3) and barrier heights (ΔE_1, ΔE_2, and ΔE_3), respectively. On the basis of the calculated values, i.e., $\Delta S_1 = 36.464$, $\Delta S_2 = 3.003$, $\Delta S_3 = 2.458$, $\Delta E_1 = 23.5$, $\Delta E_2 = 35.9$, and $\Delta E_3 = 34.6$ (the units of S and E are cal mol^{-1} K^{-1}, kcal mol^{-1}), we can obtain the ratios of k_1/k_2 and k_1/k_3 as about 10^{15} and 10^{14}, respectively. The ΔS_1 value is much larger than ΔS_2 and ΔS_3 since we find no transition states for the direct dissociation of OC(H)NO **2′** to **P₁** HCO + NO along the C−N bond, and thus ΔS_1 is the entropy difference between **2′** to **P₁**. Even if we set ΔS_1, ΔS_2, and ΔS_3 as equal, the respective k_1/k_2 and k_1/k_3 ratios are about 10^8 and 10^7. This indicates that in determining the relative abundance of the three primary products **P₁**, **P₂**, and **P₃**, the "entropic effects" may be very significant, yet the barrier height is still a predominant factor. Of course, for such a complex chemical system, it is very difficult to predict accurate branching ratios of various products, which needs detailed dynamic calculations. The results presented here are at least indicative of the predominance of **P₁** over **P₂** and **P₃**.

It is of interest to turn to why the low-lying triplet products **P₄′** ^{3}NH + CO_2 (−154.1 kcal/mol), **P₇′** HCN+$^3O_2$ (−117.7 kcal/mol), and **P₅′** HNCO+^{3}O (−114.8 kcal/mol) were not observed. In the preceding discussions, we focus on the singlet PES of the $CHNO_2$ system. Although formation of these triplet species is generally spin-forbidden, it is not impossible that they are formed via intersystem-crossing from the singlet intermediates **12**, **11**, and **3** involved in **Path P₄ (1)**, **Path P₇ (1)**, and **Path P₅ (1)**, respectively. However, even if such intersystem-crossing processes are barrierless, formation of **P₄′**, **P₇′**, and **P₅′** still cannot compete with that of **P₁** HCO + NO, **P₂** HNO + CO, **P₃** HON + CO, and **P₁₂** H + CO + NO, as can be seen from Figure 4a,b. On the other hand, the reactants CH and NO_2 can obviously be brought together on either a singlet or a triplet PES. Then a question arises: can the low-lying products **P₄′**, **P₇′**, and **P₅′** be obtained via the triplet PES? A thorough mechanistic search[9] for the triplet PES is also performed. We find that the initial triplet adduct $HCNO_2$ can also be barrierlessly formed, yet its further rearrangement to the low-lying triplet isomer OC(H)NO needs a very high barrier of about 43 kcal/mol at the CCSD(T)/6-311G(d,p)//B3LYP/6-311G(d,p) level though the conversion transition state still lies 7 kcal/mol below the reactant. This indicates that the title reaction may most possibly proceed via a singlet PES (as presented in this paper) instead of a triplet PES. Furthermore, the overall conversion barriers from triplet OC(H)NO to the triplet products **P₄′**, **P₇′**, and **P₅′** are still very large and their formation cannot at all compete with that of the HCO + NO, ^{3}HNO + CO, and ^{3}HON + CO, which can take secondary dissociation to H + CO + NO.

It should be pointed out Rim and Hershberger[6] also proposed a mechanism to qualitatively interpret their experimental result. For simplicity, their mechanism for the formation of **P₁** HCO + NO and **P₂** HNO + CO may be written as

Path P₁(1): HCONO → HCO + NO

Path P₁ (2): $HCNO_2$ → HCONO → HCO + NO

Path P₂ (1): HCONO → CON(H)O → HNO + CO

Path P₂ (2): $HCNO_2$ → HCONO → CON(H)O → HNO + CO

However, the important isomer HCONO involved in their mechanism cannot be optimized in our calculations despite numerous attempts. It is clear that their proposed mechanism is quite different from our calculated one. Note that, in order to distinguish from ours, the pathways proposed by Rim and Hershberger[6] are labeled in italics.

4. Conclusions

A detailed singlet potential energy surface of the CH + NO_2 reaction system is built up at the B3LYP and CCSD(T) (single-point) levels The main calculated results can be summarized as follows:

(1) The initial step is the side attack of CH radical on NO π bonding of NO_2 to form isomer $HCNO_2$ **1**. The terminal O-attack isomer HCONO, which was previously predicted, cannot be found. Isomer **1** then converts to the low-lying *cis*-isomer OC(H)NO **2** almost with no barrier and then **2** isomerizes to its *trans*- form **2′**very easily.

(2) Both isomers **2** and **2′** can directly dissociate to product **P₁** HCO + NO and is the most feasible dissociation channel.

Much less competitively, isomer **2′** can either dissociate to product $\mathbf{P_2}$ HNO + NO or isomerize to a weakly bound complex HON···CO **21** that dissociates very easily to product $\mathbf{P_3}$ HON + CO. The two products $\mathbf{P_2}$ and $\mathbf{P_3}$ are expected to have comparable abundance. Noticeably, product $\mathbf{P_3}$ was completely ignored by Wagal and Rim and Hershberger.

(3) The large reaction heat released from reactant **R** CH + NO_2 may causemost of the products $\mathbf{P_1}$, $\mathbf{P_2}$, and $\mathbf{P_3}$ to undergo further dissociation to the secondary product $\mathbf{P_{12}}$ H + CO + NO. Thus, reflected in the final product distributions, $\mathbf{P_{12}}$ may be the almost exclusively observable product and the remaining product $\mathbf{P_1}$, which does not take secondary dissociation, may have a very small amount of yield. The abundance of $\mathbf{P_2}$ and $\mathbf{P_{12}}$ may be even much less. The other products seem to have undetectable yields.

The calculated results are in excellent agreement with a very recent diode laser study of the CH + NO_2 reaction by Rim and Hershberger.[6] We hope our calculated mechanism may provide some useful information for understanding the NO chemistry in combustion processes.

Acknowledgment. This work is supported by the National Natural Science Foundation of China (No. 29892168, No. 20073014), Doctor Foundation of Educational Ministry, Foundation for University Key Teacher by the Ministry of Education and Key Term of Science and Technology by the Ministry of Education of China.

References and Notes

(1) (a) Miller, J. A.; Bowman, C. T. *Prog. Energy Combust. Sci.* **1989**, *15*, 287. (b) Strobel, D. F. *Planet Space Sci.* **1982**, *30*, 839.

(2) (a) Lanier, W. S.; Mulholland, J. A.; Beard, J. T. *Proc. Symp. (Int.) Combust.* **1988**, *21*, 1171. (b) Chen, S. L.; McCarthy, J. M.; Clark, W. D.; Heap, M. P.; Seeker, W. R.; Pershing, D. W. *Proc. Symp. (Int.) Combust.* **1988**, *21*, 1159.

(3) (a) Bocherel, P.; Herbert, L. B.; Rowe, B. R.; Sims, I. R.; Smith, I. W. M.; Travers, D. *J. Phys. Chem.* **1996**, *100*, 3063. (b) Jursic, B. S. *J. Phys. Chem. A* **1998**, *102*, 9225. (c) Dean, A. M.; Hanson, R. K.; Bowman, C. T. *J. Phys. Chem.* **1991**, *95*, 3180. (d) Lambrecht, R. K.; Hershberger, J. F.. *J. Phys. Chem.* **1994**, *98*, 8406. (e) Mebel, A. M.; Luna, A. M.; Lin, C.; Morokuma, K.. *J. Chem. Phys.* **1996**, *105*, 6439. (f) Marchard, N.; Jimeno, P.; Rayez, J. C.; Liotard, D. *J. Phys. Chem.* **1997**, *101*, 6077. (g) Marchard, N.; Rayez, J. C.; Smith, S. C. *J. Phys. Chem. A* **1998**, *102*, 3358. (h) Bergeaut, A.; Calvo, T.; Daugey, N.; Loison, J. C.; Dorthe, G. *J. Phys. Chem. A* **1998**, *102*, 8124. (i) Jursic, B. S. *J. Phys. Chem. A* **1999**, *103*, 1880.

(4) (a) Anderson, S. M.; Freedman, A.; Kolb, C. E. *J. Phys. Chem.* **1987**, *91*, 6272. (b) Becker, K. H.; Engelhardt, B.; Wiesen, P. *Chem. Phys. Lett.* **1989**, *154*, 342. (c) Zabarnick, S.; Fleming, J. W.; Lin, M. C. *Int. J. Chem. Kinet.* **1989**, *21*, 765. (d) Becker, K. H.; Engelhardt, B.; Geiger, H.; Kurtenbach, R.; Wiesen, P. *Chem. Phys. Lett.* **1993**, *210*, 135. (e) Hovda, N.; Hershberger, J. F. *Chem. Phys. Lett.* **1997**, *280*, 145.

(5) Wagal, S. S.; Carrington, T.; Filseth, S. V.; Sadowski, C. M. *Chem. Phys.* **1982**, *69*, 61.

(6) Rim, K. T.; Hershberger, J. F. *J. Phys. Chem. A* **1998**, *102*, 4592.

(7) Frisch, M. J.; Trucks, G. W.; Schlegel, H. B.; Scuseria, G. E.; Robb, M. A.; Cheeseman, J. R.; Zakrzewski, V. G.; Montgomery, J. A., Jr.; Stratmann, R. E.; Burant, J. C.; Dapprich, S.; Millam, J. M.; Daniels, A. D.; Kudin, K. N.; Strain, M. C.; Farkas, O.; Tomasi, J.; Barone, V.; Cossi, M.; Cammi, R.; Mennucci, B.; Pomelli, C.; Adamo, C.; Clifford, S.; Ochterski, J.; Petersson, G. A.; Ayala, P. Y.; Cui, Q.; Morokuma, K.; Malick, D. K.; Rabuck, A. D.; Raghavachari, K.; Foresman, J. B.; Cioslowski, J.; Ortiz, J. V.; Stefanov, B. B.; Liu, G.; Liashenko, A.; Piskorz, P.; Komaromi, I.; Gomperts, R.; Martin, R. L.; Fox, D. J.; Keith, T.; Al-Laham, M. A.; Peng, C. Y.; Nanayakkara, A.; Gonzalez, C.; Challacombe, M.; Gill, P. M. W.; Johnson, B.; Chen, W.; Wong, M. W.; Andres, J. L.; Gonzalez, C.; Head-Gordon, M.; Replogle, E. S.; Pople, J. A. G98W A.7; Gaussian, Inc.: Pittsburgh, PA, 1998.

(8) Chase, M. S. et al. *J. Phys. Chem. Ref. Data* **1985**, *14*, Suppl. 1.

(9) Tao, Y. G.; Ding, Y. H.; Li, Z. S.; Huang, X. R.; Sun, C. C. Unpublished results.